


 Cite this: *RSC Adv.*, 2023, 13, 12059

# Facile synthesis of layered double hydroxide nanosheets assembled porous structures for efficient drug delivery†

 Xiaohua Wang,<sup>a</sup> Haiyue Lu,<sup>a</sup> Baicheng Liao,<sup>a</sup> Gen Li<sup>a</sup> and Liyong Chen \*<sup>ab</sup>

As one of the important types of two-dimensional materials, layered double hydroxides (LDHs) have been widely used in the biomedical field as carriers for drug delivery. In this case, we propose a facile synthetic method for preparing LDH-based self-assembly structures via a metal ions-mediated zeolitic imidazolate framework-8 (ZIF-8) transformation process. The as-made hierarchical porous ZIF-8@LDHs core-shell structures and porous cages of LDHs (PC-LDHs) in drug delivery systems are used to study the loading and release of small molecular weight drugs such as doxorubicin hydrochloride (DOX) and 5-fluorouracil (5-FU). The intrinsic properties and assembly structures of both carriers are investigated in depth for their impact on slow drug release. Finally, PC-LDHs outperform ZIF-8@LDHs core-shell structures in terms of drug delivery performance under various conditions, indicating that LDH nanosheets would play a decisive role in the drug delivery process. In the drug release system, scattered LDH nanosheets with smaller sizes than their assemblies are gradually produced, allowing nanodrugs to enter cancer tissues more easily across biological barriers. This study provides the preliminary preparation for an LDH-based nanomedicine platform in the field of cancer therapy.

Received 14th February 2023

Accepted 11th April 2023

DOI: 10.1039/d3ra01000g

[rsc.li/rsc-advances](https://rsc.li/rsc-advances)

## Introduction

Drug carriers are emerging as an effective tool for providing full protection of anticancer agents including small molecular weight drugs and macromolecules of genes or proteins during the transportation process in blood vessels, allowing these anticancer agents to avoid normal tissues and be accumulated in tumours.<sup>1–4</sup> Liposomes, carbon-based materials, polymers, metal-organic frameworks (MOFs), and various inorganic materials are the main drug carriers due to their good biocompatibility, ease of surface modification, and adjustable structures for multi-site loading of drugs.<sup>5–9</sup> Additionally, the size and morphology of carriers have a significant impact on the efficiency of drug delivery to tumours.<sup>10,11</sup> For example, drug carriers exceeding 400 nm in size could confront a series of biological barriers and prevent the achievement of proper therapeutic outcomes;<sup>12</sup> traditional spherical drug carriers in circulation exhibit minimal lateral drift due to lack of tumbling and oscillating from one wall to the opposite wall in blood vessels, and thus contribute little to site-specific delivery.<sup>13</sup> As

a type of typical non-spherical drug carriers, two-dimensional (2D) nanomaterials such as graphene, transition metal dichalcogenides and layered double hydroxides (LDHs), which can overcome the aforementioned drawback of spherical carriers on account of their distinctive structures and fantastic physical/chemical properties, have drawn significant attention in the field of drug delivery.<sup>14–17</sup> Among these, LDHs are a class of ionic lamellar compounds that are widely present in nature, and thus can be considered as an intriguing candidate of drug carriers based on their ease of availability, good hydrophilicity, and low toxicity to target tissues.<sup>18</sup> In addition, guest species can be lodged in the interlayer regions, benefiting for drug loading. In the area of biomedicine, LDHs have been reported to be applied to loading chemical drugs and bio-molecules for anti-inflammatory and anti-cancer treatment by surface adsorption or intercalation into interlayer regions of LDHs.<sup>19,20</sup>

In addition to intrinsic structures and properties of drug carriers, their assembly structures may have a substantial impact on the efficiency of drug delivery. Besides the previous methods for synthesizing LDH nanosheets through coprecipitation or anion-exchange reactions, our laboratory has recently launched some research works towards development of temperature or metal ions-induced zeolitic imidazolate frameworks-67 (ZIF-67) transformation strategy for preparation of LDHs or LDHs/ZIF-67 hybrids with various assembly structures as the result of slight differences in thermodynamic stability between both materials.<sup>21,22</sup> We sought to employ zeolitic imidazolate frameworks-8 (ZIF-8) as precursors to

<sup>a</sup>Department of Pharmaceutical Engineering, Bengbu Medical College, Bengbu, 233030, China. E-mail: [lychen@bbmc.edu.cn](mailto:lychen@bbmc.edu.cn)

<sup>b</sup>Anhui Province Key Laboratory of Translational Cancer Research, Bengbu Medical College, Bengbu, 233030, China

† Electronic supplementary information (ESI) available: Experimental procedures, SEM and TEM images, UV-vis spectra, FT-IR spectra, and XRD patterns. See DOI: <https://doi.org/10.1039/d3ra01000g>



substitute ZIF-67 for synthesis of LDHs and their hybrids using a similar synthetic strategy in the research since ZIF-8 with good biocompatibility is extensively applied to studies of nanoparticle-based drug delivery platforms.<sup>23,24</sup> On the basis, to investigate the roles of mesopores and micropores respectively originated from LDH nanosheet assemblies and ZIF-8 in the drug delivery process, the small molecular weight drugs of doxorubicin hydrochloride (DOX) and 5-fluorouracil (5-FU) with different sizes to match these porous structures were used separately as therapeutic agents.<sup>25</sup> Finally, in comparison to ZIF-8@LDHs core-shell structures, LDH nanosheets assembled porous cages demonstrate better drug loading performance towards DOX; during the 5-FU loading process, ZIF-8@LDHs core-shell structures were gradually transformed into porous cages of LDHs (PC-LDHs); drug carriers with porous structures exhibit better drug sustained release performance.

## Results and discussion

### Synthesis and characterization of LDHs-based carriers

ZIF-8 nanocrystals with rhombic dodecahedral shapes were successfully prepared by a typical synthetic procedure that methanolic solutions of zinc nitrate and 1,2-dimethylimidazole were mixed and reacted in room temperature for 24 h (Fig. S1†).<sup>26</sup> However, ZIF-8 did not convert to LDHs as readily as ZIF-67 did under the same conversion conditions.<sup>22</sup> Thus, ZIF-8 nanocrystals needed to be solvothermally treated at the elevated temperature of 90 °C for 12 h in the presence of zinc nitrate to achieve partial transformation of ZIF-8, leading to the formation of ZIF-8@LDHs core-shell structures, which is confirmed by scanning electron microscopy (SEM) and transmission electron microscopy (TEM) images and X-ray diffraction (XRD) pattern (Fig. 1a–c). ZIF-8 nanocrystals were coated with a large amount of LDH nanosheets to form the ZIF-8@LDHs core-shell structures. When the reaction temperature was raised to 110 °C, only porous cages assembled with LDH nanosheets were found in the TEM and SEM images and the XRD pattern (Fig. 1e and f). These results reveal that ZIF-8 is more stable than ZIF-67 in the methanolic solution of zinc nitrate and can be converted into LDHs at higher temperature.

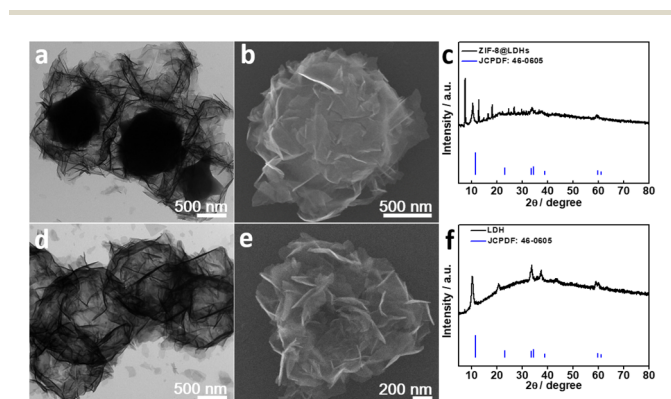


Fig. 1 TEM and SEM images and XRD patterns of (a–c) ZIF-8@LDHs core-shell structures and (d–f) PC-LDHs.

Drug carriers with large surface area and porous structures are generally contributed to their applications in drug delivery.<sup>27,28</sup>  $N_2$  sorption isotherms at 77 K were used to determine the specific surface area and average pore width of PC-LDHs structures and ZIF-8@LDHs core-shell structures. At low relative pressure, a sharp  $N_2$  adsorption in the  $N_2$  sorption isotherm of ZIF-8@LDHs core-shell structures indicates the presence of micro-porous structures originated from ZIF-8 nanocrystals.<sup>29</sup> The  $N_2$  sorption isotherm for ZIF-8@LDHs core-shell structures corresponded to a reversible type-IV isotherm associated with a well-defined H4 hysteresis loop at  $P/P_0 = 0.4$ –1.0 (Fig. 2a), which can generally be observed on the layered clay that accumulates to form meso-porous structures.<sup>30</sup> Hence, the shells assembled with LDH nanosheets were the main source of meso-porous structures in LDHs/ZIF-8 core-shell structures. Predictably, only characteristic of meso-porous structures can be found in the  $N_2$  sorption isotherm of PC-LDHs (Fig. 2b). The pore diameter distributions calculated by Barrett-Joyner-Halenda (BJH) method further confirmed the presence of micro-/meso-porous structures in LDHs/ZIF-8 core-shell structures and meso-porous structures in PC-LDHs (Fig. 2c and d). The adsorption data reveal that LDHs/ZIF-8 core-shell structures possess a very high Brunauer–Emmett–Teller (BET) surface area of  $\sim 837 \text{ m}^2 \text{ g}^{-1}$  but PC-LDHs have a relative low BET surface area of  $\sim 86 \text{ m}^2 \text{ g}^{-1}$ . Therefore, ZIF-8 is primarily responsible for the large surface area of the ZIF-8@LDHs hybrids.

### Drug loading of LDHs-based carriers

Both PC-LDHs and ZIF-8@LDHs core-shell structures were used as drug carriers to disperse into the aqueous solution of DOX with gentle stirring for 24 h in order to examine the performance of LDH nanosheets-based drug delivery platforms. Fourier transform infrared (FT-IR) spectra were gathered to determine the loading of DOX to carriers (Fig. 3). In cases of DOX, the bands at  $3523 \text{ cm}^{-1}$  and  $3305 \text{ cm}^{-1}$  might be related to N–H and O–H stretching vibrations, respectively.<sup>31,32</sup> However,

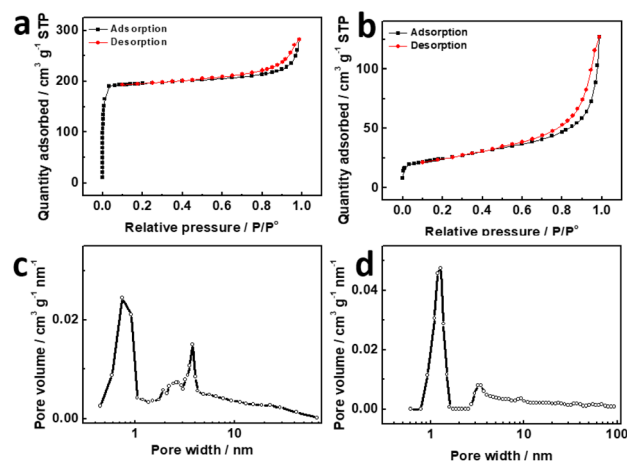


Fig. 2  $N_2$  sorption isotherms of (a) ZIF-8@LDHs core-shell structures and (b) PC-LDHs at 77 K, and pore distribution of (c) ZIF-8@LDHs core-shell structures and (d) PC-LDHs.

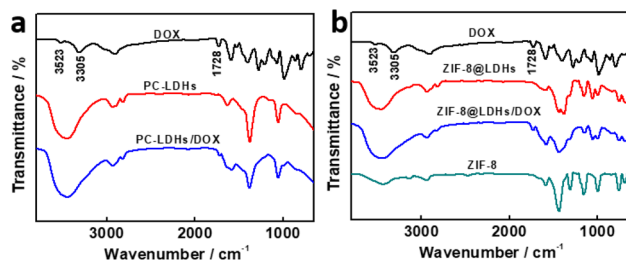


Fig. 3 FT-IR spectra of PC-LDHs (a) and ZIF-8@LDHs core-shell structures (b) with and without loading of DOX.

given the presence of a large amount of hydroxyl group in the inorganic material LDHs, a strong and broadened band attributed to O–H stretching vibrations were found in FT-IR spectra of LDHs-based materials between 3600 and 3250  $\text{cm}^{-1}$ . The loading of DOX to ZIF-8@LDHs core-shell structures (defined as ZIF-8@LDHs/DOX) can be explained by the band at 1728  $\text{cm}^{-1}$  corresponding to C=O stretching vibrations.<sup>33</sup> Similarly, the weak characteristic band of C=O stretching vibrations still was able to be found in the loaded PC-LDHs, suggesting the attachment of DOX to PC-LDH surfaces (defined as PC-LDHs/DOX).

The DOX loading on carriers was further investigated using thermogravimetric analysis. Fig. 4a showed the one primary weight loss stage of the PC-LDHs, corresponding to the decomposition of LDHs at elevated temperature. The thermogravimetry (TG) of PC-LDHs/DOX likewise exhibited a similar characteristic (Fig. 4b). Additionally, there is a loss of weight in the low-temperature region. This is due to the adsorption of numerous small molecules (such as gases and water) on PC-LDHs from the environment. PC-LDHs/DOX demonstrated a larger weight loss than PC-LDHs at this stage with a difference of around 8.6%, which is mostly attributed to desorption of the loaded drug molecules DOX. In addition, the TG of ZIF-8@LDHs core-shell structures and ZIF-8@LDHs/DOX

core-shell structures showed two primary weight loss stages, which are assigned to the decomposition of LDHs and ZIF-8 (Fig. 4c and d). Similarly, the weight loss in the initial stage is also due to the adsorbed small molecules, and the difference in weight loss ( $\sim 7.9\%$ ) between TG of ZIF-8@LDHs and ZIF-8@LDHs/DOX is mainly originated from the loaded DOX.

To precisely measure the loading amount of DOX, supernatants that were obtained after centrifugation to remove these carriers from suspensions were examined by UV-visible spectra at 500 nm (Fig. S2, S3a and b†). With the aid of a calibration curve based on the absorbance–concentration relationship, the concentration of residual DOX in supernatants was assessed using the absorbance at 500 nm. By deducting the residual DOX from the initial DOX, it is possible to determine the amount of the loaded DOX on the surfaces of carriers. In accordance with eqn (1) and (2), the DOX loading capacity (LC) and entrapment efficiency (EE) of PC-LDHs and ZIF-8@LDHs core-shell structures were successfully calculated.<sup>34</sup> Table 1 demonstrated that the LC and EE of ZIF-8@LDHs core-shell structures were marginally lower than those of PC-LDHs while the aqueous concentration of DOX was 1  $\text{mg mL}^{-1}$  and weight ratio of carriers to DOX was 4 : 1. This agrees with previous thermogravimetric results.

On the basis of LC and EE data, ZIF-8 could play a minor role in the DOX loading process. In the case of ZIF-8, ZIF-8 nanocrystals are difficultly dispersed into the aqueous solution of DOX possibly due to hydrophobic surfaces. Hence, to study the drug loading performance of ZIF-8, ZIF-8 nanocrystals were modified with polyvinyl pyrrolidone (PVP) to form hydrophilic surfaces or treated with  $\text{Co}^{2+}$  ions to produce ultra-thin LDH layers. The as-made hydrophilic ZIF-8 nanocrystals exhibited weak DOX loading performance (LC:  $<0.5\%$ ). The possible scenario is that ZIF-8 cannot provide the proper sites on the surfaces for DOX loading and DOX also cannot diffuse into small pores of ZIF-8 in size. Hence, LDHs would be mainly responsible for the drug loading.

Other than previous studies, in which the characteristic peaks of new chemical bonds were found in the FT-IR spectra of carriers after loading of DOX,<sup>33</sup> similar experimental results were not shown in the FT-IR spectra of ZIF-8@LDHs/DOX and PC-LDHs/DOX, revealing that DOX was not grafted to the surfaces of both LDHs-based carriers by chemical reactions. Electrostatic interaction could be the driving force to induce DOX adsorption on the surfaces of both carriers. Zeta potential is generally used to describe the surface charge character of nanoparticles. The zeta potential values of both PC-LDHs and ZIF-8@LDHs dispersed in water were  $\sim 15$  and 16 mV, respectively, revealing overall net positively charged LDHs-based

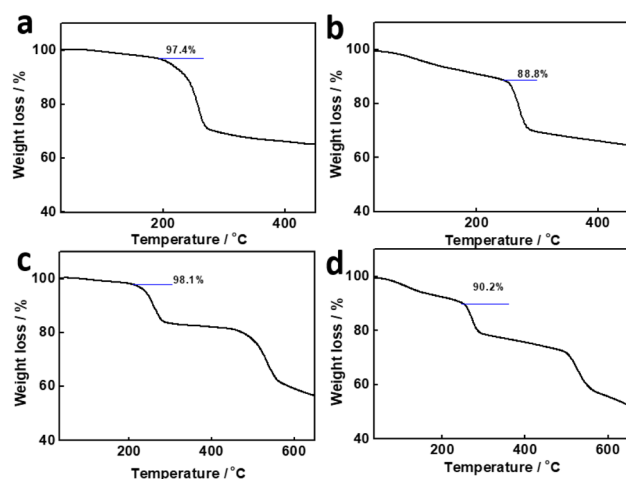


Fig. 4 TG of (a) PC-LDHs, (b) PC-LDHs/DOX, (c) ZIF-8@LDHs core-shell structures, and (d) ZIF-8@LDHs/DOX core-shell structures.

Table 1 Comparison of LC and EE of DOX in PC-LDHs and ZIF-8@LDHs core-shell structures

LC		EE	
LDHs	ZIF-8@LDHs	LDHs	ZIF-8@LDHs
10.6%	9.3%	78.3%	76.5%

carriers (Fig. 5a, c and S4†). After loading of DOX, the lower positive value for zeta potential ( $\sim 4$  and  $13$  mV) was found in PC-LDHs/DOX and ZIF-8@LDHs/DOX (Fig. 5b, d and S4†). The experimental observation is attributed to the adsorbed DOX with weak alkalinity thereby, and the negatively charged DOX molecules was loaded on the positively charged surfaces of LDH nanosheets by electrostatic interaction between them. In addition, there are a large amount of  $-\text{OH}$  groups on the surface of LDH layers and  $-\text{NH}_2$  and  $-\text{OH}$  groups from DOX, leading to the formation of hydrogen bonds that may also provide a contribution to stabilizing DOX on LDHs-based carriers.<sup>19,35</sup>

DOX was substituted with a smaller molecular molecule, 5-FU, to better understand the function of hierarchical porous structures for drug loading. Based on the absorbance at 266 nm in the UV-vis absorption spectrum, it is possible to estimate the amount of 5-FU that has been loaded into carriers (Fig. S3c, d and S5†). Experimental results revealed that both PC-LDHs and ZIF-8@LDHs showed comparable 5-FU loading performance (LC:  $\sim 8\%$ , EE:  $\sim 57\%$ ). To understand the experimental observation, the structures of ZIF-8@LDHs were further characterized after 5-FU loading. To our surprise, only diffraction peaks of LDHs were present in the XRD pattern, and ZIF-8 was absent in the SEM and TEM images of ZIF-8@LDHs core-shell structures (Fig. S6a-c†). Moreover, FT-IR spectrum of ZIF-8@LDHs/5-FU was similar to that of PC-LDHs/DOX (Fig. S6d†). These data suggest that ZIF-8 nanocrystals are etched during the process of 5-FU loading. On this basis, we speculate that 5-FU molecules firstly diffused into the interior of ZIF-8@LDHs core-shell structures from mesopores of LDH assemblies to react with ZIF-8. To further confirm the claim, the PVP-modified ZIF-8 was dispersed into the aqueous solution of 5-FU ( $1 \text{ mg mL}^{-1}$ ) to form a white suspension that completely disappeared after incubation for 24 h at room temperature, suggesting that 5-FU molecules can penetrate into ZIF-8 nanocrystals through micropores. Hence, if reaction between ZIF-8

and drug molecules cannot occur, some small molecular drugs may lodge in the micropores of ZIF-8.

### Drug release of LDHs-based carriers

One benefit of the drug delivery system is that the loaded drugs can be released gradually over a long period of time, potentially boosting the therapeutic effect. PC-LDHs/DOX and ZIF-8@LDHs/DOX were dispersed into phosphate buffer solution (PBS) with different pH value to study drug release performance. According to Fig. 6, both LDHs-based drug delivery platforms showed slow drug release performance. Within 48 h, the cumulative DOX release amounts for PC-LDHs/DOX and ZIF-8@LDHs/DOX were  $80 \pm 4.5 \text{ wt}\%$  and  $66.5 \pm 5.4 \text{ wt}\%$ , respectively, at a pH value of 7.4 and temperature of  $37^\circ\text{C}$  (Fig. 6a). Although the maximum DOX release amount is different from each other, ZIF-8@LDHs/DOX and LDHs/DOX show similar DOX release profiles, in which the drug release rate is greater in the first few hours than in the later time. The cumulative release amount was  $56.8 \pm 3 \text{ wt}\%$  for PC-LDHs/DOX and  $37.8 \pm 4.1 \text{ wt}\%$  for ZIF-8@LDHs/DOX in the first 6 h, and was increased to  $64.8 \pm 4 \text{ wt}\%$  and  $49 \pm 6.8 \text{ wt}\%$ , respectively, if the release time was further extended to 12 h. Afterwards, the cumulative release amount gradually slowed down and eventually levelled off. The possible explanation is (i) that initially a large amount of DOX molecules loaded on the surfaces of carriers result in a high drug release rate; (ii) the core-shell structure is slightly less suitable for the shuttle of guest species than the porous cages, which makes it more difficult to release drugs from core-shell structures. In addition, ZIF-8@LDHs/DOX showed the lower DOX release amount than PC-LDHs/DOX at any time within the first 12 h; after that, both carriers showed a similar DOX release rate.

In addition to the inherent properties of carriers, other factors such as pH and temperature can greatly affect the drug release performance of carriers. While the pH value of the drug

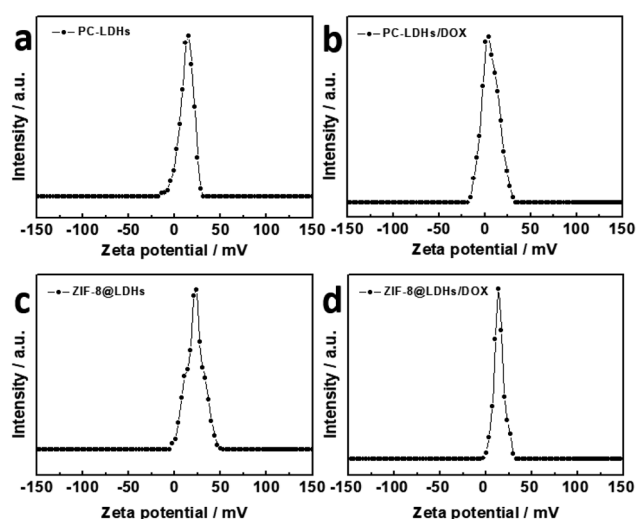


Fig. 5 Apparent zeta potential of (a) PC-LDHs, (b) PC-LDHs/DOX, (c) ZIF-8@LDHs core-shell structures and (d) ZIF-8@LDHs-DOX in water.

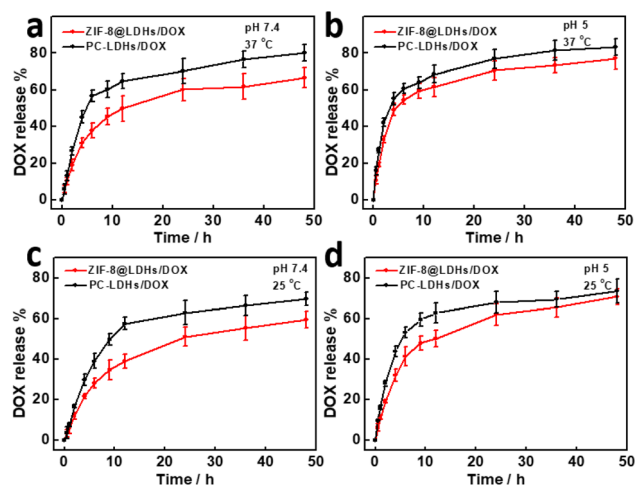


Fig. 6 Release profiles of DOX from ZIF-8@LDHs/DOX core-shell structures and PC-LDHs/DOX under the different conditions: (a) pH 7.4 and  $37^\circ\text{C}$ , (b) pH 5 and  $37^\circ\text{C}$ , (c) pH 7.4 and  $25^\circ\text{C}$ , and (d) pH 5 and  $25^\circ\text{C}$ .

release system was decreased to 5, the cumulative DOX release amounts for PC-LDHs/DOX and ZIF-8@LDHs/DOX were  $83.2 \pm 4.7$  wt% and  $77 \pm 6.1$  wt% (Fig. 6b), respectively. The release amounts were higher than those at pH 7.4. Similar experimental phenomenon also appeared in other reports on LDH-based carriers.<sup>36,37</sup> This is most likely attributed to gradually etching of LDHs by  $H^+$  ions, resulting in DOX release from the surfaces of ZIF-8@LDHs or PC-LDHs. To further confirm the speculation, when PC-LDHs were dispersed into PBS with pH 5 and kept at 37 °C for a week, few PC-LDHs were collected by centrifugation, suggesting that PC-LDHs are etched into very small fragments and even completely dissolved. In addition, at 25 °C both PC-LDHs/DOX and ZIF-8@LDHs/DOX showed a lower cumulative release amount of DOX within 48 h compared to the temperature at 37 °C (Fig. 6c and d). This could be greatly dependent on an endothermic process of drug release.<sup>38</sup>

The drug release performance of small 5-FU molecules loaded PC-LDHs was also studied at 37 °C and various pH levels. Other than DOX, 5-FU was rapidly released from PC-LDHs at different pHs more than 60 wt% in the first 0.5 h (Fig. 7a), suggesting that LDHs have no slow release performance to 5-FU. However, after that, the drug release rate of 5-FU greatly decreased. On the basis, if 5-FU loaded LDHs were incubated in water for 0.5 h and collected by centrifugation, the treated LDHs/5-FU could exhibit slow drug release performance. As shown in Fig. 7b, a curve of the treated PC-LDHs/5-FU for 5-FU release with a similar profile to that of DOX release from LDHs/DOX was observed at different pHs. Hence, the treated PC-LDHs/5-FU can be considered as sustained-release drugs although LC of 5-FU in LDHs was not high after treatment.

The therapeutic efficacy is generally affected by the size of carriers. ZIF-8@LDHs core-shell structures and PC-LDHs difficultly overcome biological barriers and are unable to access to tumour tissues due to their large size. After DOX release from PC-LDHs/DOX for 48 h at 37 °C and pH 7.4, more scattered small nanosheets that were able to overcome the biological barriers and possibly facilitated the chemotherapy efficacy were found (Fig. S7†). The PC-LDHs were ground and then dispersed in water before being sonicated for 12 h to produce the scattered LDH nanosheets that were employed as carriers for drug delivery (Fig. S8†). In comparison to the LDH nanosheets assembled porous cages, the scattered LDH nanosheets showed a similar loading performance towards DOX with 10.1 wt% LC and 78.4% EE, but a higher drug release rate with  $62.3 \pm$

1.4 wt% cumulative release amount of DOX in the first 8 h. Therefore, porous structures in our case did not affect the loading of small molecular drugs but rather enhanced the chemotherapeutic efficacy of tumours to some extent due to the slower drug release rate as well as the drug nanocarriers of LDH nanosheets produced during the drug release process.

## Conclusions

In summary, we have successfully prepared low-cost porous LDHs-based assemblies, such as ZIF-8@LDHs core-shell structures and PC-LDHs, using a  $Co^{2+}$  ions-induced ZIF-8 transformation strategy at different temperatures. Both LDHs-based assemblies with high biocompatibility were utilized as carriers to load small molecular drugs with different sizes, such as DOX and 5-FU, in order to study the impact of porous structures on their drug slow release performance. ZIF-8 nanocrystals with micropores in the ZIF-8@LDHs core-shell structure did not contribute anymore when large-size DOX molecules were loaded, but ZIF-8 was entirely dissolved by etching when small-size 5-FU molecules were loaded. The mesopores originating from assemblies of LDH nanosheets can limit the shuttling of guest species, and thus improve slow drug release of DOX and 5-FU. During the process of drug release, PC-LDHs are allowed to gradually convert into small-size separated nanosheets by etching of  $H^+$  ions, potentially improving the LDHs-based nanomedicine platform for cancer therapy efficacy by cellular uptake.

## Author contributions

Conceptualization: Liyong Chen and Xiaohua Wang; methodology, visualization, and formal analysis: Xiaohua Wang, Haiyue Lu, Baicheng Liao, and Gen Li; writing – original draft preparation: Xiaohua Wang, Liyong Chen; funding acquisition, supervision, writing – review & editing: Liyong Chen.

## Conflicts of interest

The authors declare no competing financial interest.

## Acknowledgements

The authors thank the financial support from the Natural Science Foundation of Anhui Province of China (Grant No. 2108085MB47), and Academic Program Foundation of Anhui Province for Top Talents of Universities (Grant No. gxbjZD2022040).

## Notes and references

- 1 H. S. El-Sawy, A. M. Al-Abd, T. A. Ahmed, K. M. El-Say and V. P. Torchilin, *ACS Nano*, 2018, **12**, 10636–10664.
- 2 W. Zhang, M. Wang, W. Tang, R. Wen, S. Zhou, C. Lee, H. Wang, W. Jiang, I. M. Delahunty, Z. Zhen, H. Chen, M. Chapman, Z. Wu, E. W. Howerth, H. Cai, Z. Li and J. Xie, *Adv. Mater.*, 2018, **30**, e1805557.

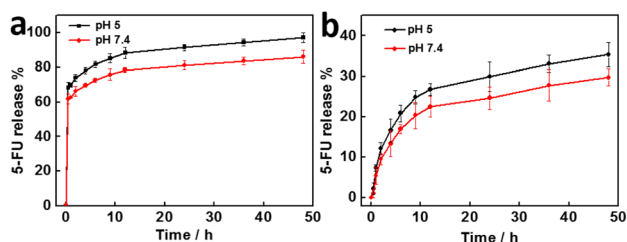


Fig. 7 Release profiles of 5-FU at 37 °C under different pHs from (a) PC-LDHs/5-FU and (b) PC-LDHs/5-FU with treatment in water.

- 3 H. Xiang, Y. Wu, X. Zhu, M. She, Q. An, R. Zhou, P. Xu, F. Zhao, L. Yan and Y. Zhao, *J. Am. Chem. Soc.*, 2021, **143**, 11449–11461.
- 4 G. Chen, I. Roy, C. Yang and P. N. Prasad, *Chem. Rev.*, 2016, **116**, 2826–2885.
- 5 J. Shi, P. W. Kantoff, R. Wooster and O. C. Farokhzad, *Nat. Rev. Cancer*, 2016, **17**, 20–37.
- 6 H. Wang, Q. Chen and S. Zhou, *Chem. Soc. Rev.*, 2018, **47**, 4198–4232.
- 7 S. Lv, M. Sylvestre, A. N. Prossnitz, L. F. Yang and S. H. Pun, *Chem. Rev.*, 2021, **121**, 11653–11698.
- 8 Z. Zhou, M. Vazquez-Gonzalez and I. Willner, *Chem. Soc. Rev.*, 2021, **50**, 4541–4563.
- 9 W. Chen, C. A. Glackin, M. A. Horwitz and J. I. Zink, *Acc. Chem. Res.*, 2019, **52**, 1531–1542.
- 10 S. Wilhelm, A. J. Tavares, Q. Dai, S. Ohta, J. Dvorak, H. F. Dvorak and W. C. W. Chan, *Nat. Rev. Mater.*, 2016, **1**, 1–12.
- 11 A. Albanese, P. S. Tang and W. C. Chan, *Annu. Rev. Biomed. Eng.*, 2012, **14**, 1–16.
- 12 T. Sun, Y. S. Zhang, B. Pang, D. C. Hyun, M. Yang and Y. Xia, *Angew. Chem., Int. Ed.*, 2014, **53**, 12320–12364.
- 13 P. Decuzzi, S. Lee, B. Bhushan and M. Ferrari, *Annu. Rev. Biomed. Eng.*, 2005, **33**, 179–190.
- 14 L. Mei, S. Zhu, W. Yin, C. Chen, G. Nie, Z. Gu and Y. Zhao, *Theranostics*, 2020, **10**, 757–781.
- 15 Z. Gu, S. Zhu, L. Yan, F. Zhao and Y. Zhao, *Adv. Mater.*, 2019, **31**, e1800662.
- 16 T. Liu, C. Wang, X. Gu, H. Gong, L. Cheng, X. Shi, L. Feng, B. Sun and Z. Liu, *Adv. Mater.*, 2014, **26**, 3433–3440.
- 17 A. K. Gaharwar, L. M. Cross, C. W. Peak, K. Gold, J. K. Carrow, A. Brokesh and K. A. Singh, *Adv. Mater.*, 2019, **31**, e1900332.
- 18 Q. Wang and D. O'Hare, *Chem. Rev.*, 2012, **112**, 4124–4155.
- 19 X. Bi, H. Zhang and L. Dou, *Pharmaceutics*, 2014, **6**, 298–332.
- 20 A. Hakeem, G. Zhan, Q. Xu, T. Yong, X. Yang and L. Gan, *J. Mater. Chem. B*, 2018, **6**, 5768–5774.
- 21 L. Chen, H. Wang, X. Shen, Y. Zhang, D. Li and C. Duan, *Inorg. Chem. Front.*, 2019, **6**, 1415–1421.
- 22 L. Chen, J. Wang, X. Shen, X. Li and C. Duan, *Inorg. Chem. Front.*, 2019, **6**, 3140–3145.
- 23 A. Yuan, C. Hao, X. Wu, M. Sun, A. Qu, L. Xu, H. Kuang and C. Xu, *Adv. Mater.*, 2020, **32**, e1906580.
- 24 Z. Wang, X. Tang, X. Wang, D. Yang, C. Yang, Y. Lou, J. Chen and N. He, *Chem. Commun.*, 2016, **52**, 12210–12213.
- 25 E. Ranjbar, H. Namazi and M. Pooresmaeil, *Int. J. Biol. Macromol.*, 2022, **201**, 193–202.
- 26 L. Chen, Y. Peng, H. Wang, Z. Gua and C. Duana, *Chem. Commun.*, 2014, **50**, 8651–8654.
- 27 N. Ahmad, H. A. Younus, Z. Gaoke, K. Van Hecke and F. Verpoort, *Adv. Mater.*, 2019, **31**, e1801399.
- 28 K. Khaletskaya, J. Reboul, M. Meilikhov, M. Nakahama, S. Diring, M. Tsujimoto, S. Isoda, F. Kim, K. Kamei, R. A. Fischer, S. Kitagawa and S. Furukawa, *J. Am. Chem. Soc.*, 2013, **135**, 10998–11005.
- 29 G. Leofantia, M. Padovanb, G. Tozzolac and B. Venturellic, *Catal. Today*, 1998, **41**, 207–219.
- 30 N. C. Burtch, H. Jasuja and K. S. Walton, *Chem. Rev.*, 2014, **114**, 10575–10612.
- 31 Y. Sun, Y.-L. Sun, L. Wang, J. Ma, Y.-W. Yang and H. Gao, *Microporous Mesoporous Mater.*, 2014, **185**, 245–253.
- 32 W. L. Ye, Y. P. Zhao, H. Q. Li, R. Na, F. Li, Q. B. Mei, M. G. Zhao and S. Y. Zhou, *Sci. Rep.*, 2015, **5**, 14614.
- 33 K. Shanthi, K. Vimala, D. Gopi and S. Kannan, *RSC Adv.*, 2015, **5**, 44998–45014.
- 34 N. Zhang, N. Feng, X. Xin, J. Zhang, D. Wu, Q. Jiang, T. Yu, M. Gao, S. Zhao, H. Yang and Q. Tian, *Nanomedicine*, 2022, **45**, 102592.
- 35 L. Wang, H. Xing, S. Zhang, Q. Ren, L. Pan, K. Zhang, W. Bu, X. Zheng, L. Zhou, W. Peng, Y. Hua and J. Shi, *Biomaterials*, 2013, **34**, 3390–3401.
- 36 G. Li, Y. Fan, L. Lin, R. Wu, M. Shen and X. Shi, *Sci. China Chem.*, 2021, **64**, 817–826.
- 37 J. Liu, L. Sun, L. Li, R. Zhang and Z. P. Xu, *ACS Appl. Mater. Interfaces*, 2021, **13**, 7115–7126.
- 38 H. Peng, B. Cui, W. Zhao, X. Zhao, Y. Wang, Z. Chang and Y. Wang, *New J. Chem.*, 2016, **40**, 1460–1470.